Supporting Information

Pak et al. 10.1073/pnas.1318705110

SI Methods

Protein Expression and Purification. Cells were fermented using a 15 L Biostat C bioreactor (Sartorius Stedim Biotech) at 30 °C to an OD_{600} of ~4 to 5, after which expression was induced with 2 mM IPTG for 3.5 h. The harvested cells were resuspended in buffer containing 20 mM Hepes, pH 8.0, 300 mM NaCl, and EDTA-free protease inhibitor (Roche), and lysed by an EmulsiFlex (Avestin) at 15,000 psi or a BeadBeater (Bio Spec Products). Cellular debris was removed by centrifugation at 15,000 × *g* for 15 min. Membranes were isolated by ultracentrifugation for 1 h at 140,000 × *g*. Membrane pellets were first washed in a low detergent concentration buffer [20 mM Hepes, pH 8.0, 300 mM NaCl, 10% (vol/vol) glycerol and 0.02% (wt/vol) n-dodecyl β-D-maltoside (β-DDM)] and then solubilized in the same buffer containing 1% (wt/vol) of α- or β-DDM for 1 to 1.5 h at 4 °C. After centrifugation, the supernatant was incubated with Ni-NTA agarose (Qiagen), in the presence of 10 mM imidazole, for 1 to 2 h. Washes and elutions were performed in steps (15 mM, 25 mM, 50 mM, and 300 mM imidazole), and the eluted ZneA was dialyzed overnight against 20 mM Hepes, pH 8.0, 300 mM NaCl, 10% glycerol, and 0.05% α- or β-DDM. Following dialysis, ZneA was further purified by using a TSK-3000 column (Tosoh Bioscience) equilibrated with 20 mM MES, pH 6.0, 100 mM NaCl, 10% glycerol, and 0.05% α- or β-DDM.

Reconstitution of ZneA and Transport Assay. A dried lipid film of *E. coli* polar lipid extract (Avanti Polar Lipids) was resuspended in 20 mM Hepes, 150 mM NaCl, pH 7.5, followed by sonication to create small unilamellar vesicles (SUVs). Purified ZneA was added to the SUV suspension at a protein:lipid mass ratio of 1:15 and at a final β-DDM concentration of 1.6 mM. After incubation for 1.5 h under gentle agitation at 4 °C, the detergent was removed using Bio-Beads SM-2 (Bio-Rad). After reconstitution, the proteoliposomes were collected by centrifugation at 25,000 × *g* for 30 min at 4 °C, resuspended in 20 mM Hepes, 150 mM choline chloride, pH 7.9, containing 1 mM of metal ion, and submitted to three freeze/thaw cycles. Excess metal ion was removed by two cycles of centrifugation at 25,000 × *g* for 30 min at 4 °C. The ΔpH (inside-alkaline) was established by the addition of proteoliposomes to 2 mL of 20 mM Hepes, 150 mM NH_4Cl, pH 6.9. Choline chloride/NH_4Cl salts were used to increase the strength of ΔpH across the membrane (48). Metal ion transport was detected by monitoring the fluorescence of FluoZin-3 (Molecular Probes) present in the medium at a final concentration of 1 μM.

Membrane Potential-Driven Transport Assay. For ΔΨ-driven transport assays, proteoliposomes were generated as described for ΔpH experiments, with the following exceptions. The protein-to-lipid mass ratio during reconstitution was 1:50 and, after centrifugation, the proteoliposome pellet was resuspended in 20 mM Hepes, 150 mM KCl [for ΔΨ (inside-negative)] or 150 mM NaCl [for ΔΨ (inside-positive)], 1 mM of $ZnCl_2$, pH 7.9. Proteoliposomes were diluted in assay buffer containing 20 mM Hepes, 150 mM NaCl [for ΔΨ (inside-negative)] or 150 mM KCl [for ΔΨ (inside-positive)], 1 μM FluoZin-3, pH 7.9. A total of 5 μM valinomycin was added to the proteoliposome/assay buffer mixture to generate ΔΨ. Assays were performed in duplicate, showing similar results.

Data Collection, Structure Determination, and Refinement. All diffraction images were collected at 100 K, and reduced and scaled by using HKL2000 (1). For both datasets, an R_{free} test set of ~2,000 reflections was randomly generated by using PHENIX (2). The molecular replacement solutions were subjected to several cycles of simulated annealing (Cartesian, starting temperature 5,000 K), followed by coordinate and individual B-factor refinement, using PHENIX. For the low-pH crystal form, TLS refinement was performed by manually selecting three TLS groups corresponding to the docking domain, porter domain, and transmembrane domain. In addition, all twofold non-crystallographic symmetry (NCS) combinations between monomers belonging to the different trimers were tested, and the pairs that resulted in the lowest R and R_{free} (A–D, B–E, and C–F) were NCS-restrained for refinement. The resulting difference Fourier electron density maps revealed strong density for unmodeled side chains and loops. The strongest peaks in the difference Fourier electron density maps corresponded to Zn(II) at the proximal site. Coordinate, individual B-factor and occupancies were refined for Zn(II) ions at the proximal site, resulting in near full occupancy (average occupancy, 0.97 ± 0.02) and refined B-factors (average B, 107.2 ± 6.0 $Å^2$) that are comparable to the average B-factor for the protein (average B, 77.7 $Å^2$). Model rebuilding was performed in Coot, and the structure was refined at 3.0 Å with R of 27.9% and R_{free} of 30.5%. The structure exhibited good stereochemistry, with 90.2% of residues in the most favored region, and 8.8% of residues in the allowed region of the Ramachandran plot.

Analysis of the intensity statistics, as implemented in PHENIX Xtriage, from all low-pH crystal form datasets collected to date, suggest the presence of twinning in this crystal form. To explore the possibility of twinning, we refined the structure in *C*2 and *P*1 in PHENIX using a variety of pseudomerohedral twinning laws. In the case of the *C*2 space group, pseudomerohedral twinning laws applicable when β is equal to 90° were tested. Simulated annealing (Cartesian, starting temperature of 5,000 K), coordinate and individual B-factor refinement was performed. In all cases of twinning refinement, the electron density maps were highly model-biased, and the difference Fourier electron density maps showed no density for omitted loops, side chains, and Zn (II) ions. Therefore, refinement with a twinning operator was not performed for the low-pH crystal form.

The high-pH crystal form was solved by molecular replacement by using PHASER (3), using a partially refined low-pH ZneA monomer as the molecular replacement search molecule. Three monomers (one biological trimer) are found in the asymmetric unit, corresponding to ~60% solvent content in the unit cell. The high-pH crystal form was refined in a similar manner to that of the low-pH crystal form described earlier, with the exception that Ramachandran restraints were applied. In addition, no NCS restraints were applied during refinement. The strongest peaks in the difference Fourier electron density maps corresponded to Zn(II) at the proximal site, followed by Zn(II) at the distal site. Coordinate, individual B-factor and occupancies were refined for Zn(II) ions at the proximal site and the distal site, resulting in full occupancy and refined B-factors (average B, 124.3 ± 20.8 $Å^2$) that are comparable to the average B-factor for the protein (average B, 122.4 $Å^2$). Intensity statistics for the high-pH crystal form dataset did not suggest the presence of twinning. The structure was refined at 3.7 Å with R of 22.9% and R_{free} of 28.3%. The use of Ramachandran restraints during refinement with PHENIX improved the stereochemistry of the model, and the final model exhibits 93.4% of residues in the most favored, and 6.4% of residues in the allowed, region of the Ramachandran plot.

1. Otwinowski Z, Minor W (1997) Processing of X-ray diffraction data collected in oscillation mode. *Methods Enzymol* 276:307–326.
2. Adams PD, et al. (2010) *PHENIX*: A comprehensive Python-based system for macromolecular structure solution. *Acta Crystallogr D Biol Crystallogr* 66(pt 2):213–221.
3. McCoy AJ, et al. (2007) Phaser crystallographic software. *J Appl Cryst* 40(pt 4):658–674.
4. Notredame C, Higgins DG, Heringa J (2000) T-Coffee: A novel method for fast and accurate multiple sequence alignment. *J Mol Biol* 302(1):205–217.

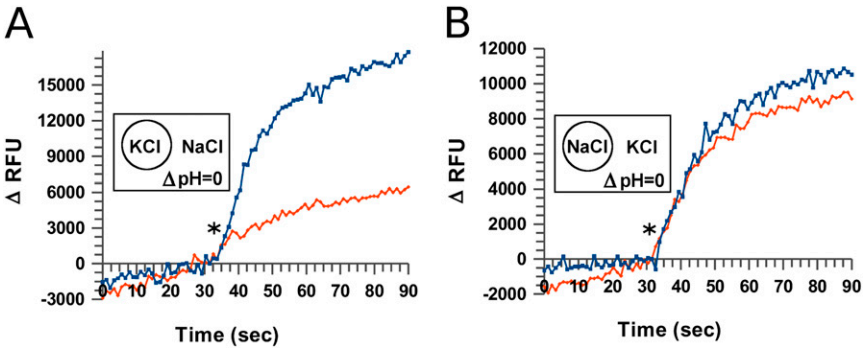

Fig. S1. Membrane potential driven efflux of Zn(II). (*A*) ΔΨ (inside-negative) or (*B*) ΔΨ (inside-positive) was generated by the addition of 5 μM valinomycin (black asterisk) to the assay buffer containing equal amounts of ZneA proteoliposomes (blue) or control liposomes (red). The change in FluoZin-3 fluorescence [i.e., change in relative fluorescence units (ΔRFU)] was determined relative to the fluorescence immediately before the addition of valinomycin. A single representative measurement from two independent measurements is shown.

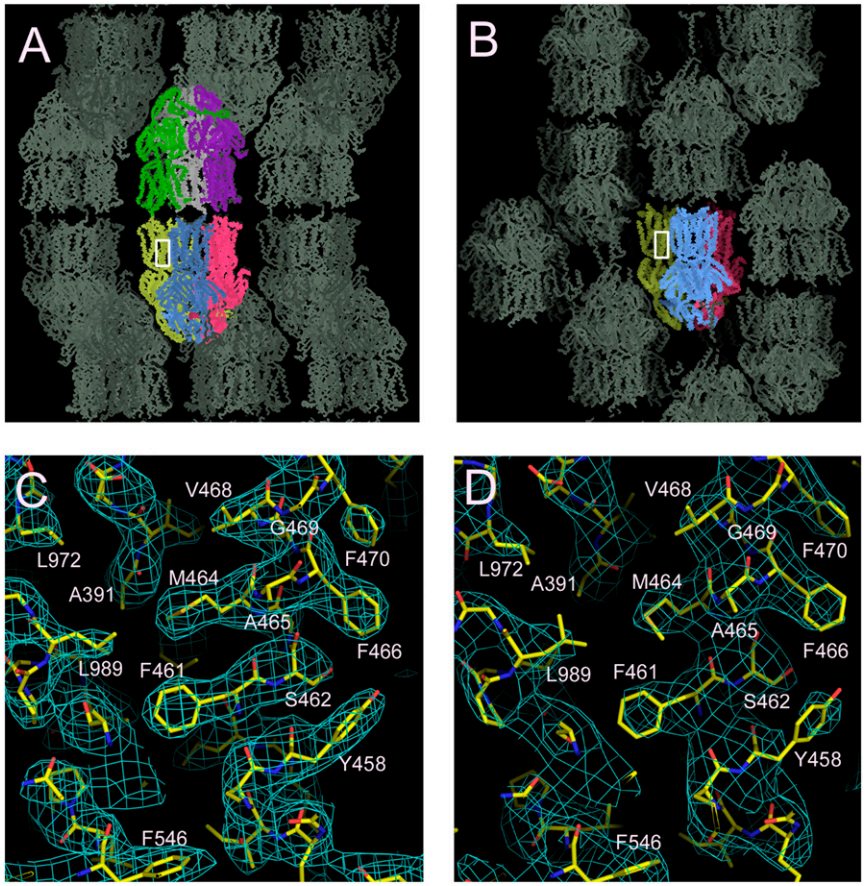

Fig. S2. Crystal packing and 2mFo-DFc electron density for ZneA. (*A*) Low-pH and (*B*) high-pH crystal forms of ZneA. Each protomer in the asymmetric unit is depicted in a different color. Symmetry-related molecules are depicted in dark gray. Representative 2mFo-DFc electron density for the low-pH (*C*) and high-pH (*D*) crystal forms, contoured at 1σ. Regions shown are depicted in *A* and *B* with a white rectangle.

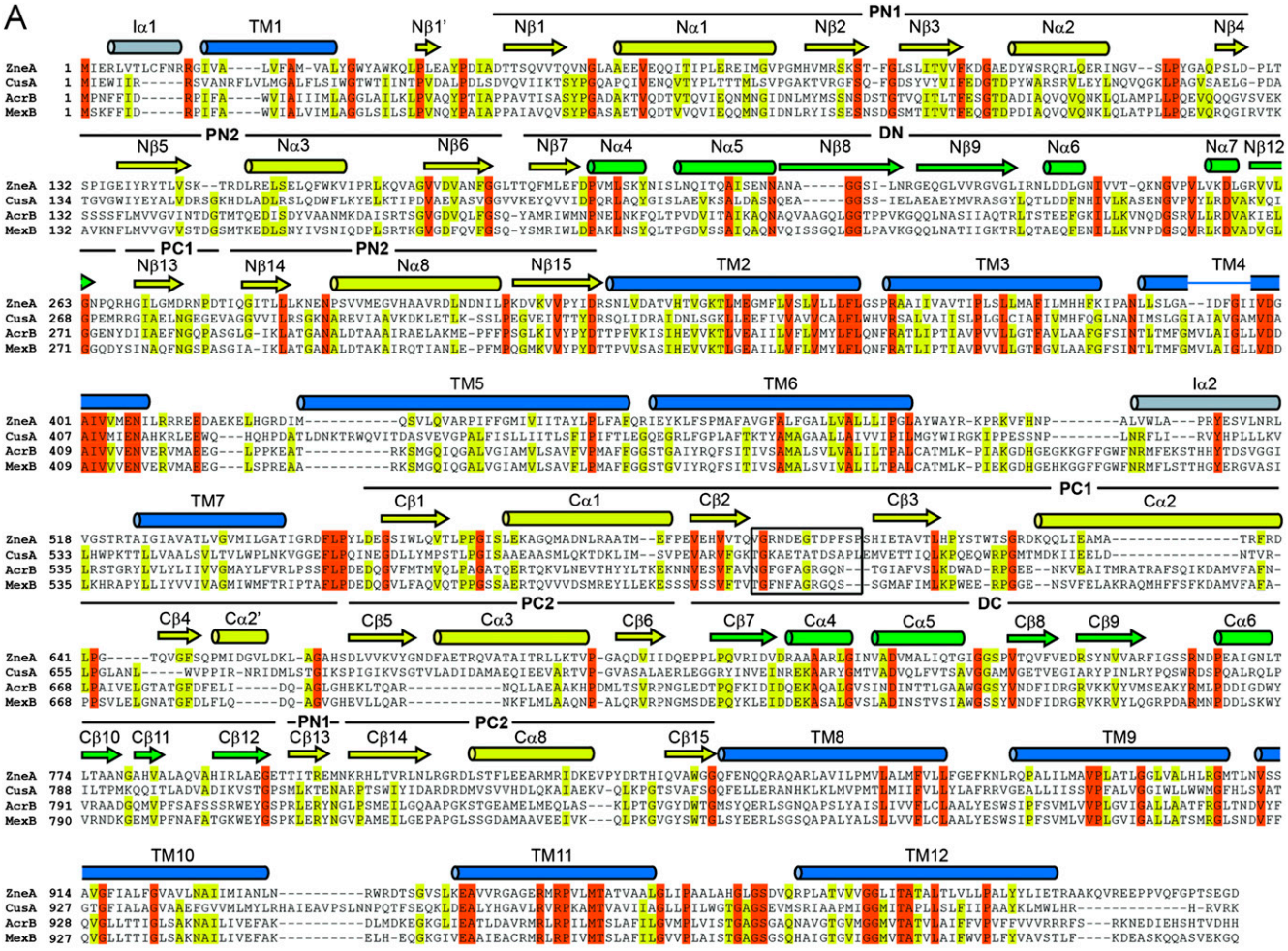

B

	Proximal Site					Distal Site			Specificity
ZneA	E136	D602	E610	D654	D658	D172	E599	E72	Divalent metals Zn(II)
CzcA	E138	D619	D627	L672	E676	E183	I616	V72	Divalent metals Cd(II), Zn(II), Co(II)
CnrA	E138	D650	D650	M695	E699	D207	L639	A72	Divalent metals Co(II), Ni(II)
CusA	W138	D617	E625	N668	M672	E176	T614	T72	Monovalent metals Cu(I), Ag(I)
AcrB	F136	-----	I626	-----	-----	D174	-----	N68	Hydrophobic/ amphiphilic drugs

Fig. S3. Sequence alignment of resistance–nodulation–cell division (RND) proteins. (*A*) Sequences of RND efflux pumps where structures have been determined (*Cupriavidus metallidurans* ZneA, *Escherichia coli* CusA, *E. coli* AcrB, and *Pseudomonas aeruginosa* MexB) were aligned by using T-Coffee (4). Orange and yellow highlighted sequences represent 100% and 75% sequence identity, respectively. Secondary structure elements for ZneA are shown and named according to those of AcrB, and colored in blue (transmembrane helices), yellow (porter domain), green (docking domain), and gray (cytoplasmic). The access loop is enclosed in a black box. (*B*) Proximal and distal site sequence of *C. metallidurans* CH34 ZneA compared with the corresponding sequences of *C. metallidurans* CH34 CzcA and CnrA. For *E. coli* CusA and AcrB, structurally equivalent residues to ZneA are shown. Conserved residues are shown in dark blue, with similar residues shown in light blue. Residues of ZneA that have no structurally equivalent residue in AcrB are depicted with dashed lines.

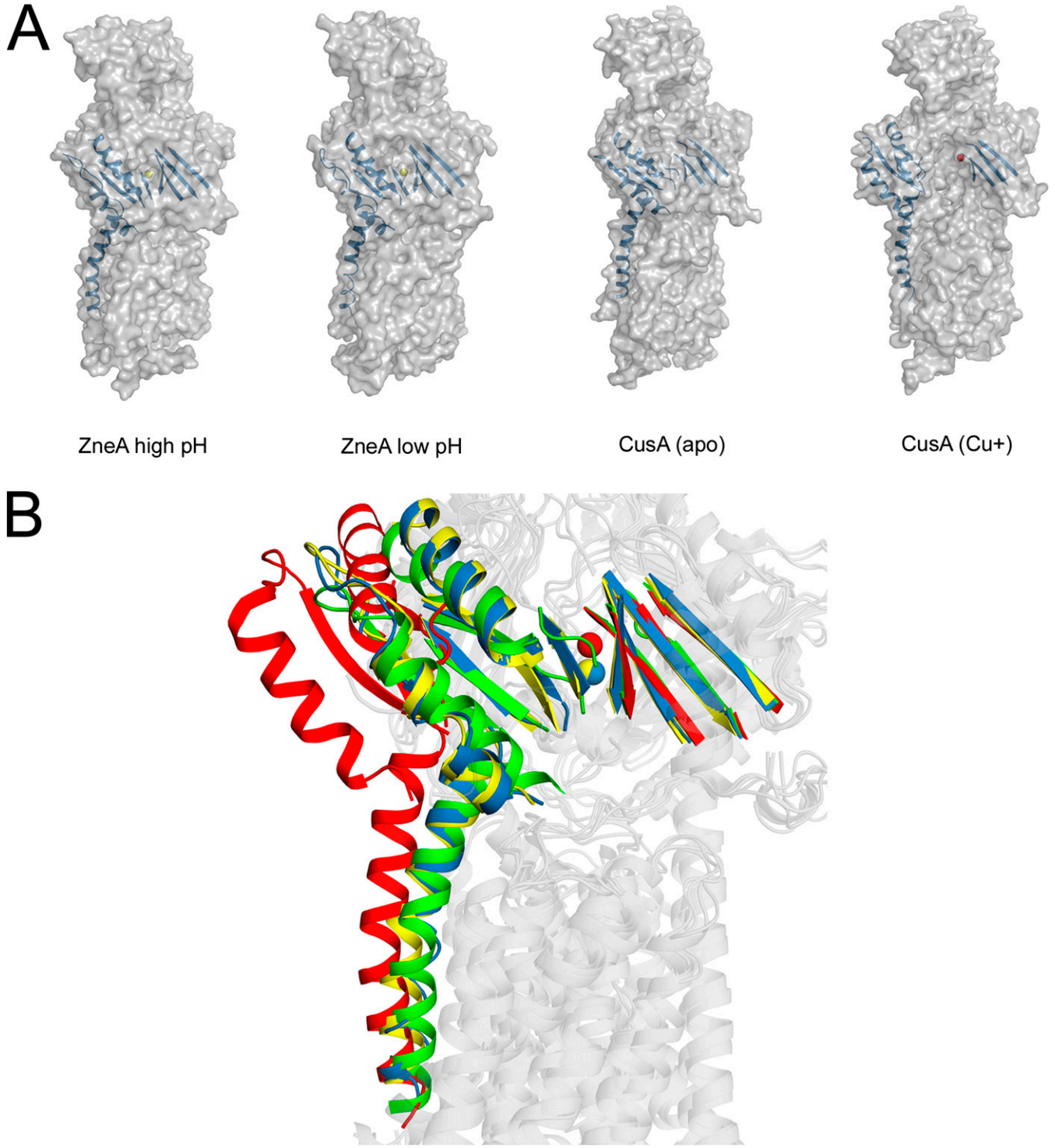

Fig. S4. Conformational flexibility of the porter domain cleft in the presence and absence of substrate. (*A*) Structures of ZneA (high pH), ZneA (low pH), CusA (*apo*), and CusA [Cu(I)-bound] are shown in surface representation (gray). Selected residues are shown in cartoon representation (blue). Zn(II) and Cu(I) are shown as spheres in yellow and red, respectively. The orientation shown for all structures is similar. For both ZneA structures, the chain A protomer is shown. (*B*) Close-up of the structural alignment between ZneA and CusA. Selected residues and bound Zn(II) or Cu(I) shown in *A* are depicted for ZneA (high pH) in blue, ZneA (low pH) in yellow, CusA (*apo*) in green, and CusA [Cu(I)-bound] in red. The orientation shown is similar to that of *A*.

Table S1. Crystallographic statistics for ZneA

Data collection and refinement statistics	ZneA (pH 7.5, high pH)	ZneA (pH 5.2, low pH)
Data collection		
Source	ALS 8.3.1	APS 23-ID-B
Space group	*C*2	*C*2
Cell dimensions		
a, *b*, *c*, Å	215.34, 127.07, 163.33	223.63, 129.06, 392.37
α, β, γ, °	90, 93.12, 90	90, 94.62, 90
Wavelength, Å	1.1159	1.0332
Resolution, Å	20–3.7 (3.83–3.7)	20–3.0 (3.11–3.0)
Completeness, %	97.5 (98.7)	98.5 (99.6)
Redundancy	2.5 (2.4)	2.7 (2.7)
R_{sym}, %	12.3 (67.8)	10.9 (66.1)
$I/\sigma I$	6.8 (1.5)	10.0 (1.8)
Refinement		
Resolution, Å	20–3.7	20–3.0
R_{work}/R_{free}	22.9/28.3	27.9/30.5
No. of reflections	41,916	213,992
No. of atoms	22,061	44,020
β-factors, Å^2		
Protein	122.4	77.7
Ligand	124.3	107.2
rmsd		
Bond lengths, Å	0.003	0.004
Bond angles, °	0.817	0.860